ChemSusChem

Chemistry–Sustainability–Energy–Materials

Chemistry Europe

European Chemical Societies Publishing

Accepted Article

Title: An efficient electrochromic supercapacitor based on solution-processable nanoporous poly(tris[4-(3,4-ethylenedioxythiophene) phenyl]amine)

Authors: Yaokang Lv, Xing Yang, Weishi Du, Peihua Ma, Antoine Bonnefont, Dominic Wright, Laurent Ruhlmann, and Cheng Zhang

To be cited as: *ChemSusChem* 10.1002/cssc.202000941

Link to VoR: https://doi.org/10.1002/cssc.202000941

WILEY-VCH

10.1002/cssc.202000941

An efficient electrochromic supercapacitor based on solution-processable nanoporous poly(tris[4-(3,4-ethylenedioxythiophene) phenyl]amine)

Yaokang Lv, [a,b] Xing Yang,[a] Weishi Du,[a] Peihua Ma,[c] Hu Wang,[a] Antoine Bonnefont,[b] Dominic. S. Wright, *[d] Laurent Ruhlmann*[b] and Cheng Zhang*[a]

Abstract: A new green-synthetic route to the tris[4-(3,4-ethylenedioxythiophene)phenyl]amine (TEPA) monomer has been developed and the molecular structure of TEPA determined by a single-crystal X-ray study for the first time. Solution-processable nanoporous poly(tris[4-(3,4-ethylenedioxythiophene)phenyl]amine) (PTEPA) was prepared via chemical-oxidative polymerization in a microemulsion. Based on the distorted structure of TEPA found in the solid-state, we speculate that dendritic PTEPA has a distorted three-dimensional conformation with multiple twisted channels and pores which are narrowed and blocked by the bifurcation and distortion of PTEPA, which is consistent with the observed hierarchical pore structure. As a cathode material, PTEPA exhibits a discharge capacity of 89.5 mAh/g in the initial cycle with a very sloping two-stage discharge curve and relatively stable cycling performance. Beyond excellent energy storage properties, PTEPA also shows relatively good electrochromic performance. On this basis, an efficient all-solid-state electrochromic supercapacitor (ECSC) with good electrochromic performance and high energy storage capacity (13.3 mF cm^{-2}) was assembled based on PTEPA and nanoporous graphene films. During the charging and discharging processes, the color of the ECSC changes between yellow-green and steel-blue. Thus, the energy storage level of the ECSC can be monitored by the corresponding color changes. The fabricated ECSC may have practical applications, for example, in self-powered electrochromic smart windows.

Introduction

The Electrochromic devices (ECDs), such as electrochromic smart windows, which can efficiently adjust light transmission through reversible color and transparency changes under an external voltage,[1-4] and supercapacitors (SCs), which are advanced electrochemical energy storage devices characterised for their high power density and short charging times,[4-7] have similar working mechanisms and device structures. As a result, there is the interesting prospect of the integrating energy storage and electrochromic functions into one device. As a promising smart device, such electrochromic supercapacitors (ECSCs) have attracted considerable interest over the past decade.[8-14] In comparison with traditional ECDs, ECSCs not only have the function of energy storage, but also can act simultaneously as a smart energy monitor, indicating the state of energy storage capacity through color changes. In addition, ECSCs are also expected to overcome problems concerning external power sources and the limited range of application of conventional ECDs.

Conjugated polymers have been widely viewed as an attractive option for electrode materials due to their adjustable band gaps, large theoretical specific capacitances, good electrical conductivity, high elemental abundance, light weight, and tunable mechanical flexibility.[1,15] Recently, H. Cheng's group synthesized several novel solution-processable electrochromic conjugated polymers,[15b,15c] and G. R. Reynolds's group evaluated the electrochromic properties of a series of homopolymers based on dioxythiophene with differently solubilizing side chains. [15d,15e] J. Y. Lee et al. synthesized a novel quinoxaline-based conjugated donor-acceptor random copolymer, which is highly soluble in organic solvents and exhibits excellent electrochromic performance.[15f] K. Sheng et al. fabricated a new electrochromic device consisting of poly(3,4-(2,2-dimethylpropylenedioxy)thiophene) and tungsten trioxide (WO_3) films.[15g] S. Ming et al. designed a new conjugated polymer poly(BT-Th-EDOT) which can be applied in ECSCs,[15h] and Q. Guo et al. fabricated two new ECSCs based on poly(indole-6-carboxylicacid)/TiO_2 and poly(indole-5-carboxylic acid)/WO_3 nanocomposites.[13,14] Among these reported conjugated polymers, many triphenylamine(TPA)-based polymers, which possess ultrafast electron-transfer rate constants and good hole-transporting ability, have been intensively studied as electrode materials for organic batteries and SCs.[16-23] In addition, a large number of TPA-based polymers also exhibit electrochromic behavior during redox processes that have potential applications in ECDs.[22-36] In order to improve the charge carrier transport properties and structural stabilities of polymer chains, some thiophene derivatives, such as 2,2'-bithiophene and 3,4-ethylenedioxythiophene (EDOT), have been incorporated within the polymer backbone as "bridge" linkages. A series of monomers consisting of a TPA core substituted by thiophene derivatives

[a] Dr. Y. Lv, X. Yang, W. Du, H. Wang, Prof. C. Zhang*
International Sci. & Tech. Cooperation Base of Energy Materials and Application, College of Chemical Engineering
Zhejiang University of Technology
Hangzhou 310014, P. R. China
E-mail: czhang@zjut.edu.cn; yaokanglv@zjut.edu.cn
[b] Dr. A. Bonnefont, Dr. Y. Lv*, Dr. L. Ruhlmann*
Institut de Chimie (UMR au CNRS n°7177)
Université de Strasbourg
4, rue Blaise Pascal CS 90032, F-67081 Strasbourg Cedex, France
E-mail: lruhlmann@unistra.fr
[c] P. Ma
Shaoxing Jinye Environmental Protection Technology Co., Ltd.
No.173, Zhenghai Road, Binhai Industrial Zone, Keqiao District, Shaoxing, 312073, China.
[d] Prof. D. S. Wright*
Department of Chemistry
University of Cambridge
Lensfield Road, Cambridge CB2 1EW, UK.
E-mail: dsw1000@cam.ac.uk

Supporting information for this article is given via a link at the end of the document, CCDC 1988890

10.1002/cssc.202000941

were synthesized recently, and the resulting polymers possess good electrochemical stability and various electrochromic properties.[31-36] Tris[4-(3,4-ethylenedioxythiophene)phenyl]amine (TEPA) is one of reported monomers, which has been synthesized via the Stille cross-coupling reaction.[31,37] M. Chahma et al.[37] and K. Idzik et al.[38] have prepared poly(tris[4-(3,4-ethylenedioxythiophene)phenyl]amine) (PTEPA) films by electrochemical polymerization and found that they have significant electroactivity and reasonable redox stability, although these films are insoluble in all common solvents. C. Xu et al.[31] firstly studied the electrochromic properties of PTEPA films, which exhibit four different colors (yellow green, green, blue and steel-blue) upon applied stepwise oxidations from -0.4 to 0.95 V. This property indicates that PTEPA is a potential candidate as an electrode material for ECSC. Nevertheless, this material still has several drawbacks that hinder its practical application. Firstly, because of the toxicity of organotin reagents, conventional Stille coupling reactions are not suitable for environmentally-friendly production,[39] alternative "greener" synthesis procedures for the TEPA monomer should be investigated. Secondly, electrochemically polymerized PTEPA films can not be dissolved in common organic solvents, their molecular weights were not determined and the processability was limited.[40-43] Last but not least, there has been no report on the energy storage properties of PTEPA, not to mention the application of this material in ECSCs.

In view of the issues mentioned above, here we have developed a novel synthetic route to the TEPA monomer and determined its molecular structure in the solid state for the first time. We also report the preparation of PTEPA via a chemical oxidative polymerization in a microemulsion. These nanoporous polymers exhibit excellent energy storage properties and are soluble in chloroform with a number-average molecular weight of 13843 g/mol. Thin electrochromic films were prepared by drop casting, and an ECSC with good electrochromic performance and high energy storage capacity was assembled based on PTEPA. The smart visual monitoring of the energy storage state of the ECSC is provided by means of the observed color tuning during the charging-discharging process.

Results and Discussion

Synthesis and Structure of TEPA

In 2007, M. Chahma et al. reported the synthesis of TEPA through a Stille coupling reaction between tris[4-bromophenyl]amine and 2-tributylstannyl-3,4-ethylenedioxythiophene. However, because of the toxicity of organotin reagents and the difficulties in separating organotin by-products from target products, this synthetic pathway his problematic in large-scale synthesis. As shown in Scheme 1, we obtained a light yellow powder of TEPA via a Suzuki-Miyaura cross-coupling reaction between tris[4-(4,4,5,5-tetramethyl-1,3,2-dioxaborolan-2-yl)phenyl]amine and 2-iodo-3,4-(ethylenedioxy)thiophene, the overall yield of TEPA through this four step synthetic route can be reached 55%. Compared with the previous route, our new route is greener and uses environmentally benign reagents. It will therefore be more suitable for industrial production.

The purity of TEPA produced by our method was confirmed by elemental analysis, NMR, MS and FT-IR spectra (Figs. S1-S3). In addition, the simulated powder XRD pattern is identical to that of authentic samples of TEPA (Fig. S4). The molecular structure of TEPA was determined via sXRD analysis. This compound crystallizes in the monoclinic centrosymmetric space group $P2_1/c$, with three (chemically identical) crystallographically independent molecules within the unit cell.

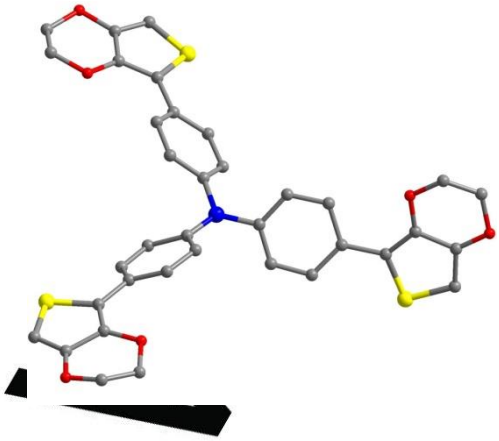

Figure 1. Molecular structure of TEPA, H-atoms have been omitted for clarity (red = O, blue = N, gray = C, yellow = S), and only one of the three independent molecules in the unit cell is shown.

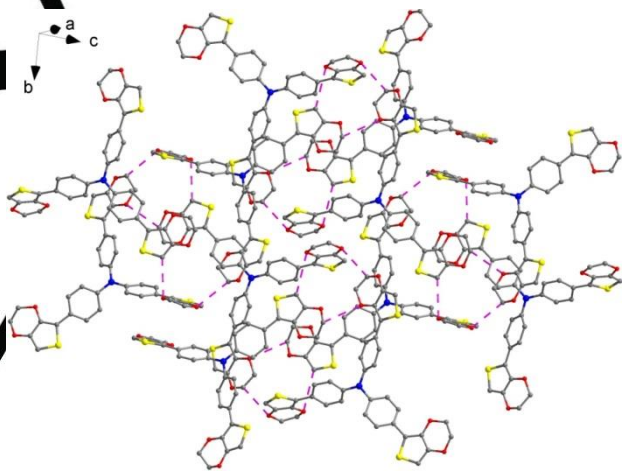

Figure 2. Two-dimensional layers of TEPA molecules linked by C—H···O intermolecular hydrogen bonds.

As depicted in Fig. 1, molecules of TEPA have a propeller-like TPA core with each 'blade' being an EDOT group and with the central N-atom being nearly trigonal planar [C-N-C over the three independent molecules being in the range of 118.5(10)-122.2(9)°]. The carbon atoms at the 2-position of the thiophene rings of the EDOT groups are bonded to the para position of the triphenylamine groups of the TPA core. As shown in Fig. 2, C—H···O intermolecular hydrogen bonds connect adjacent molecules and form two-dimensional layers within the lattice (Table S2), which further extend into a 3D supramolecular structure through Van der Waals interactions (Fig. 3). As shown in Fig. 4 and Table S3, molecules of TEPA have a highly distorted arrangement. The three phenyl groups of the TPA core within individual molecules are not in the same plane, with the dihedral

10.1002/cssc.202000941

angles between the neighboring phenyl groups of TPA core being in the range of 59.9-74.5° (Fig. 4a). In addition, the phenyl and thiophene rings are also not co-planar, with the dihedral angles between these rings being in the range of 18.6-23.3° (Fig. 4b). These features are important because, in general, planarity and the resulting conjugation are strongly related to the band gap and conductivity of polymers, while the planarity of monomer units determines the planarity of the conjugated polymer to a large extent.[46-48] Small conformational differences may produce large band-gap effects in conjugated polymers.[49] The structure of the TEPA monomer is therefore not only related to the conformation of PTEPA but also to its physical properties.

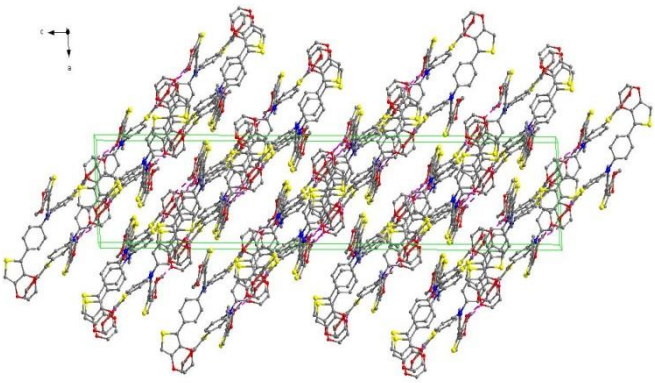

Figure 3. Molecular packing of TEPA.

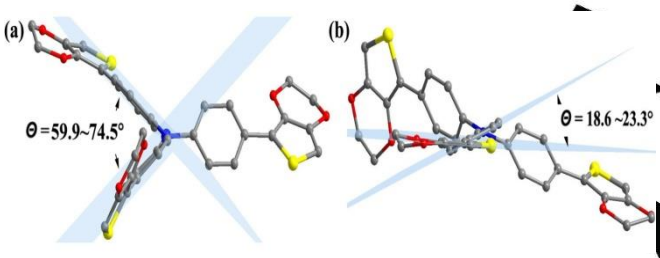

Figure 4. Key dimensions of the TEPA monomer units, indicating the distortion of the polymer building blocks.

In some previous reports, due to the lack of accurate structural informations, monomeric units have been approximated to completely planar, 'star-shaped' building blocks.[19,23] As a result, it has been assumed that the highly porous polymers observed result from the aggregation of monomers into cyclic units which build together into planar, honey-comb arrangements e.g., in poly[1,3,5-tris(4-diphenylamino-phenyl)benzene] which has been shown to possess a highly porous structure. As represented in Fig. 5a, the TEPA monomer is in reality not a completely planar building block but is slightly pyramidalised at the central N1 atom with respect to the terminal C atoms (C1A, C1B, C1C), which will form C-C bonds to other monomer units upon polymerisation. As shown in Table S4, the distances from the central N atoms to the terminal C atoms over all three independent molecules in the unit cell are in the range of 0.808-0.817 nm, while the associated C-N-C angles are in the range of 117.4-122.9°.

Fig. 5b shows two possible assemblies of TEPA, although it is possible to assemble a nanoring through three connected TEPA molecules (shown on the left of Fig. 5b) which would form the previously proposed honeycomb sheet arrangement, the inherent distortion of the building blocks of TEPA are, we believe, more likely to result in the formation polymer chains (Fig. 5b, right). In this case polymerization of TEPA would result in irregular spiral channels (Fig. 5c) instead of the ordered columnar channels which would occur in a honeycomb structure. As shown in Fig. 5d, cross-linking of this arrangement will give a three-dimensional porous dendritic structure. As the degree of polymerization increases, the affect of the bifurcation and distortion of PTEPA will be accumulation throughout the structure of the polymer, while the pores and channels in PTEPA will be also gradually twisted and blocked by the external branches. This less porous structure is consistent with porosity measurements of PTEPA (section 3.2). It was reported that polytriphenylamine(PTA) displays negligible microporous structure with a very small surface area,[19a,20] which, it was proposed, may be due to the difficulty in building a porous honeycomb structure using a monomer with shorter connecting groups.[19a] Based on our hypothesis, we speculate that the structure of PTA contains similar twisted pores and channels to that proposed for PTEPA.

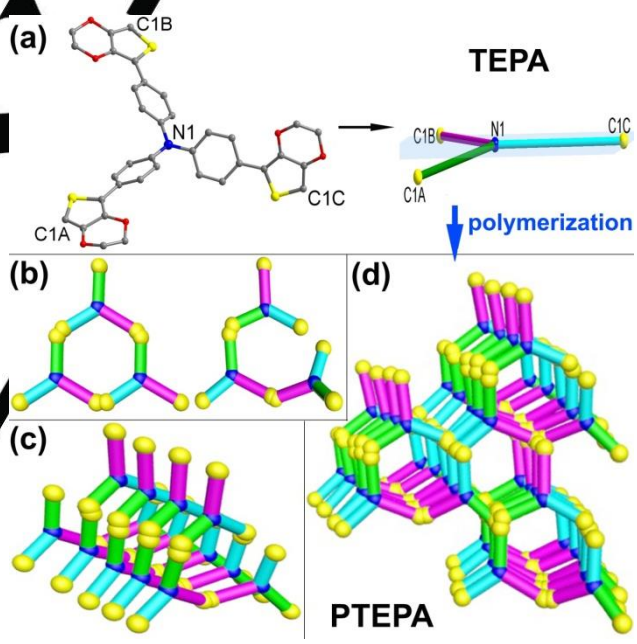

Figure 5. (a) Schematic representation of the TEPA monomer as a building block, (b) two possible assemblies of PTEPA, (c) a possible spiral channel of PTEPA, (d) a possible porous polymer structure of PTEPA.

Synthesis and Structure of PTEPA

Dendritic homopolymer and copolymer films based on TEPA have been synthesized via electropolymerization in previous reports.[21,37] But all of these polymers exhibit insolubility in conventional organic solvents, which introduces difficulties for large-scale production. Microemulsion polymerization has been regarded as a simple and reliable process for preparation of nanostructured conjugated ploymers and oligomers.[50-53] In this work, a PTEPA powder was prepared via micelle-induced self-

10.1002/cssc.202000941

assembly and in situ polymerization of TEPA monomers. As a surfactant, DTAB forms micelles between the stirred aqueous and organic biphasic system during the microemulsion polymerization, TEPA diffuses into the micelles, where the oxidizing agent oxidizes it and subsequent polymerization occurs. As shown in Fig. 6, the obtained PTEPA powder is composed of irregular nanoparticles, most of which loosely agglomerated together. Nitrogen adsorption-desorption experiments were conducted to further explore the microstructure of the PTEPA. As presented in Fig. 6d, the PTEPA exhibits a type IV isotherm with hierarchical pore structure: an obvious hysteresis loop between the sorption curve and the desorption curve suggests the presence of mesopores.[54,55] A significant rise in the sorption curve in the high pressure region ($0.80 < P/P_0 < 0.95$) indicates the presence of macropores, and a sharp uptake at low pressures ($P/P_0 < 0.01$) is a characteristic feature for microporous materials.[56,57] The Brunauer–Emmett–Teller (BET) surface area of PTEPA calculated in the low pressure region ($0.009 < P/P_0 < 0.05$) of the isotherm is 67 m^2/g, and the total pore volume was calculated as 0.25 cm^3/g (P/P_0 = 0.992) for PTEPA. Pore size distributions calculated from desorption branches by the Barrett-Joyner-Halenda (BJH) model are given in Fig. 6e. PTEPA display typical hierarchical pore size distribution with a highest peak centering at ca. 1.94 nm, a lower peak centering at ca. 7.98 nm and micropores smaller than 1.53 nm. The average pore radius is 6.8 nm. In addition, micropore distribution of PTEPA analyzed by the Horvath-Kawazoe method (Fig. 6f) reveal that PTEPA has a narrow micropore size distribution with median pore width of 1.07 nm. These results prove that PTEPA is nanoporous, which is in accord with the schematic polymer structure of PTEPA (Fig. 5). The macropores and mesopores in PTEPA are mainly derived from the removed solvent and surfactant after polymerization, while the micropores stem from the porous framework of PTEPA. Inherent nanopores make the numerous active sites of PTEPA accessible by electrolyte ions during electrochemical processes. This may benefit the performance in electrical energy storage systems.

Interestingly, this PTEPA powder can be dissolved in chloroform, the number-average molecular weight (M_n) of PTEPA is 13843 g/mol, with a PDI of 2.24, determined using GPC. The solubility of PTEPA facilitates its processability for coating or printing, thin films of PTEPA on ITO glass substrates were prepared by drop casting from a 1 g/L chloroform solution of PTEPA and dried in air at room temperature. As observed in Fig. 6c, these films exhibit a rough surface containing widely distributed nanopores.

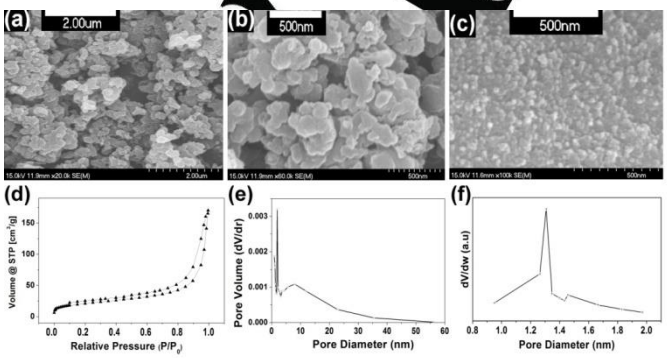

Figure 6. SEM images of PTEPA powder taken at a magnification of (a) 20k and (b) 60k; (c) SEM image of a PTEPA film; (d) Nitrogen adsorption–desorption isotherms of PTEPA powder; (e) BJH pore size distribution from the desorption isotherms of PTEPA; (f) microporous pore size distribution in PTEPA calculated from the adsorption isotherms.

Electrochemical Energy Storage Performance

The electrochemical energy storage performances of a PTEPA electrode as the cathode was investigated in a 2032 coin-type half-cell. As shown in Fig. 7a, CV profiles of the electrode exhibit pairs of broad redox peaks located at 3.69 V *vs.* Li/Li^+ (oxidation) and 3.37 V *vs.* Li/Li^+ (reduction). The separation of the redox waves in PTEPA is approximately 0.32 V, which is a slightly narrower than that previously reported for the polytriphenylamine (PTPA) electrode (0.35 V).[19a] The symmetric peak shape of the oxidation and reduction peaks of PTEPA demonstrates its capacitance characteristic. The charge-discharge behavior of the PTEPA electrode was explored at 20 mA/g between 2.5 V and 4.3 V. As shown in Fig. 7b, the PTEPA electrode exhibits a discharge capacity of 89.5 mAh/g in the initial cycle with two sloping voltage stages. The high voltage stage between the voltage of 4.1 V and 3.3 V is attributed to the redox reaction of TPA moieties of the PTEPA, which provides discharge capacity of about 62 mAh/g, while the other lower stage between 2.8 V and 2.6 V is probably related to the EDOT moieties, which provides a discharge capacity of about 27.5 mAh/g. Compared with other reported active materials, PTEPA exhibits a more sloping discharge curve without a stable discharge voltage plateau, which indicates that it is more suitable for applications in SCs than in batteries.

The cycling performance of the PTEPA electrode was examined at a constant current of 20 mA/g during a 50 cycle test and the results are shown in Fig. 7c. It is found that the discharge capacity of PTEPA decreases from its initial 89.5 mAh/g to 84.9 mAh/g after 50 cycles, with about a 5% loss of capacity. The cycling stability of the PTEPA electrode is better than that of PTPA electrodes reported in the literature.[19] The relatively stable cycling performance of PTEPA can be attributed to its nanoporous structure which reduced potential electrochemical decomposition and morphological change during the repeated charge-discharge processes. As shown in Fig. 7d, PTEPA exhibits relatively low coulombic efficiency in the initial charge-discharge process that is related to formation of an solid electrolyte interface (SEI) membrane on the lithium anode. With increase in cycling, the coulombic efficiency increased, reaching 98.3% at the 50th cycle. This increase can be attributed to improved wetting of the electrodes and to an improvement of the SEI properties upon cycling.

Electrochemical measurements show that the PTEPA film on ITO exhibits mainly a Faradaic pseudocapacitive behavior in 1M H_2SO_4 aqueous solution. As shown in Fig. 7e. CV profiles of the PTEPA electrode exhibit a pair of broad redox waves centered at 0.67 V *vs.* Ag/AgCl (oxidation) and 0.39 V *vs.* Ag/AgCl (reduction), with good reversibility. As shown in Fig. 7f., the galvanostatic charge-discharge profiles show a significant IR drop at the beginning of the discharge process, followed by slow discharge process (0.8 V to 0.2 V), the potential sharply reverts to the original value afterward. The coulombic efficiency of the PTEPA film is about 43%. However, since the thin PTEPA film is easily detached from the ITO substrate during the charge and

10.1002/cssc.202000941

discharge process, it is difficult to determine the film mass and to calculate specific capacity accurately.

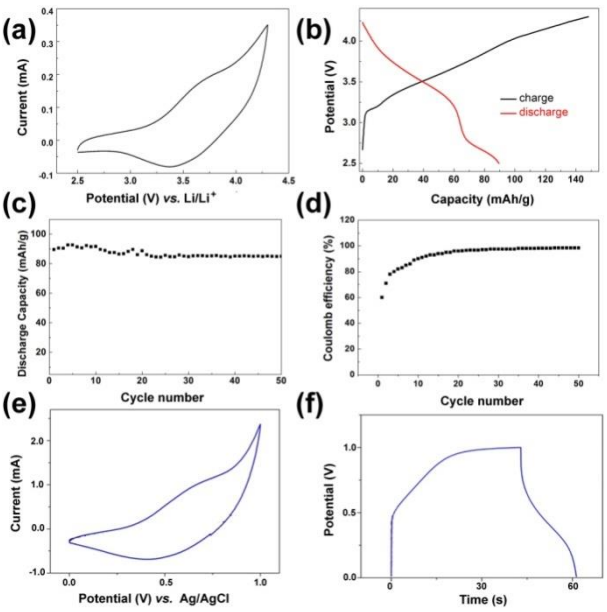

Figure 7. (a) CV curve of the PTEPA electrode in $LiPF_6$ EC/DMC (v/v, 1:1) electrolyte versus Li/Li^+, at a scan rate of 1 mV/s; (b) Initial charge-discharge curves of the PTEPA electrode at a current density of 20 mA/g; (c) Cycling stability of the PTEPA electrode at a current density of 20 mA/g; (d) Coulomb Efficiency of the PTEPA electrode; (e) CV curve of the PTEPA film in 1 mol/L H_2SO_4 aqueous solution versus Ag/AgCl, at a scan rate of 100mV/s (f) GCD curves of the PTEPA film in 1 mol/L H_2SO_4 aqueous solution at approximately 10 A/g.

Spectroelectrochemistry Studies

Spectroelectrochemical analysis was used to study the electrochromic properties of the PTEPA films on ITO. Vis/NIR and NIR transmission spectra of the PTEPA film at different potentials (-0.5 to 1.0 V) are shown in Fig. 8a. When a -0.5 V voltage was applied, the PTEPA film in its reduced state exhibited a yellow-green color with two absorption bands. The absorption band centered at 440 nm was attributed to the π–π* transition and the broad absorption band between 560 nm and 1050 nm was assigned to the charge transfer band from the TPA moiety to the EDOT moiety.[31] Upon increasing the applied potential, the intensity of absorption peak around 440 nm was decreased, while the broad absorption peak at higher wavelength increases, leading to a color change to steel-blue at the fully oxidized state (1.0 V).

In order to characterize the optical contrast (ΔT%) and switching properties of the PTEPA film, dynamic electrochromic experiments were studied at 440 nm and 660 nm. The square wave potential method was used between −0.4 V and 1.0 V at regular intervals of 5 s. As shown in Fig. 8b, the ΔT% was found to be 23.97% at 440 nm and 14.29% at 660 nm, which were are slightly lower than that of electroploymerized PTEPA films (26.84% at 440 nm and 17.03% at 660 nm),[31] as shown in Fig. S11, the coloration efficiency values of the PTEPA film are calculated to be 80.6 cm^2/C at 440nm and 122.8 cm^2/C at 660 nm (see ESI). In addition, the switching time of the PTEPA film was found to be 0.96 s for coloring and 1.89 s for bleaching at 440 nm (Fig. 8c), and 0.67 s for coloring and 2.89 s for bleaching at 660 nm (Fig. 8d). These times are longer compared to electroploymerized PTEPA film. These phenomena can be attributed to the relatively low polymerization degree of the drop-casted film. As summarized in Table S5, solution-processable PTEPA still exhibits relatively short coloring times, which may in part be due to the nanoporosity of PTEPA, resulting in relatively high interface area and small diffusion length. The reasonable optical contrast and the fast switching properties make PTEPA a promising electrochromic material and will be beneficial to its application in ECSCs.

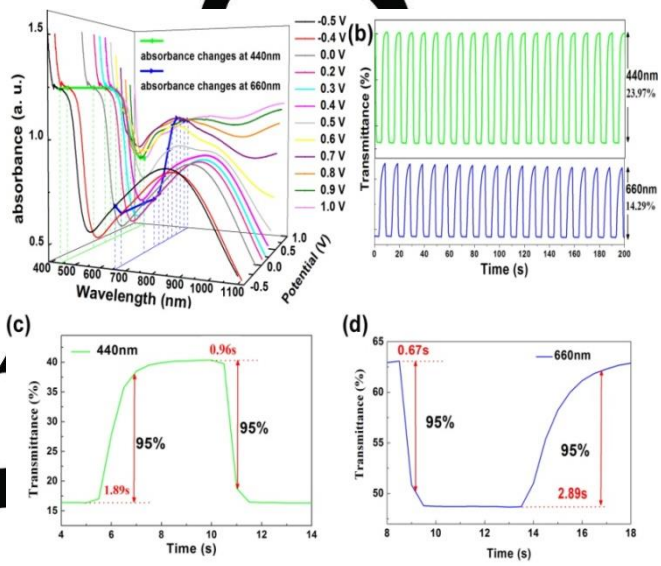

Figure 8. (a) Spectroelectrochemical spectra of PTEPA films with different applied potentials between -0.4 V and 1.0 V; (b) Transmittance-time profiles of PTEPA films at 440 nm and 660 nm between -0.4 and 1.0 V with a residence of 5 s; (c) Switching response for PTEPA films monitored at 440 nm; (d) Switching response for PTEPA films monitored at 660 nm.

Performance of the Solid-state ECSC

As shown in Fig. 9a, an all-solid-state ECSC prototype was constructed based on PTEPA and nanoporous graphene films (Fig. S6). Nanoporous graphene films and PVA/H_2SO_4 gel electrolyte were prepared according to reported methods.[6] The detailed fabrication process of the ECSC is described in the ESI. The CV curves of the ECSC in the voltage window of -0.8 V~0.2 V are shown in Fig. 9b at different scan rates, which exhibit a quasi-rectangular shape at sweep rates from 0.01 to 0.10 V/s, indicating ideal capacitance behavior. However, this rectangular behavior changes at sweep rates of 0.20 V/s, suggesting resistance-like electrochemical behavior. The GCD curves of the ECSC were almost linear (Fig. 9d) and exhibit good symmetry. The IR drop of the ECSC increased from 7.9 mV at 0.015 mA/cm^2 to 76 mV at 0.12 mA/cm^2, such a low IR drop indicates that the device has high electron transfer efficiency and low equivalent series resistance. The latter is estimated to be around 175 Ω cm^2 by using electrochemical impedance spectroscopy (see ESI). The area specific capacitance of the device can reach a maximum of 13.3 mF/cm^2 with a current density of 0.015 mA/cm^2, but the specific capacitance of the ECSC significantly decays with increase in the current density (Fig. 9c). When the current density

10.1002/cssc.202000941

is increased to 0.03 mA/cm^2, the area specific capacity decreased to 10.9 mF/cm^2, when the current density is increased to 0.12 mA/cm^2, the area specific capacity dropped to 7.2 mF/cm^2, while when the current density increased to 0.30 mA/cm^2, the area specific capacity dropped to 5.4 mF/cm^2. These capacitance values are in good agreement with the value of 9.2 mF cm^{-2} determined by electrochemical impedance spectroscopy.

Since energy storage and electrochromism rely on the same electrochemical processes, the color of the ECSC changed between yellow-green and steel-blue reversibly during the charging and discharging processes. When the device was charged to 0.2 V, the color of the ECSC was steel-blue (see inset to Fig. 9d). In the opposite direction, when the device was discharged to -0.8 V, the color of this ECSC changed to yellow green (inset to Fig. 9d). Therefore, the energy storage level of ECSC can be monitored by the corresponding color changes.

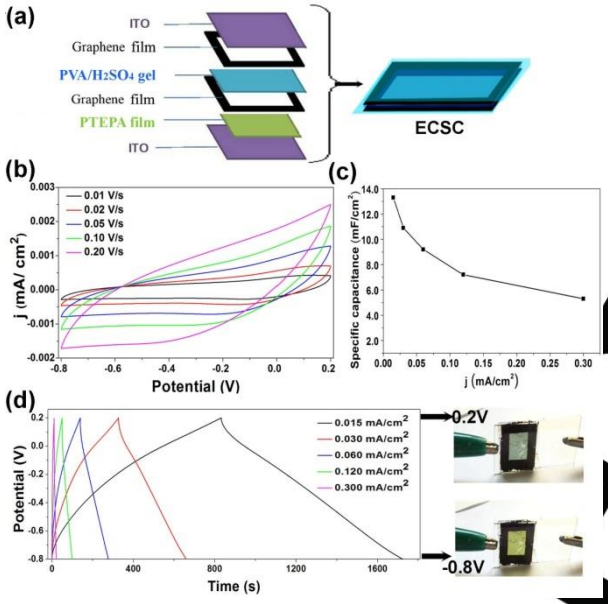

Figure 9. (a) The assembly structure of the all-solid-state **ECSC**; (b) CV curves of the **ECSC** in the voltage window of -0.8 V~0.2 V at different scan rates; (c) Specific capacitance of the **ECSC** at different current densities; (d) Charge-discharge curves of the **ECSC** at different current densities and the corresponding digital photograph of the device.

As summarized in Table 1, the maximum specific capacitance of the ECSC is higher than that of other reported electrochromic supercapacitors. It should be noted that the CV and GCD curves of our ECSC were very different to that of PTEPA. Nanoporous graphene films have excellent conductivity and high electric double-layer capacitance. In the case of the ECSC fabricated with a PTEPA and nanoporous graphene films, both the oxidation and reduction peaks of PTEPA disappear from the CV curves and the corresponding GCD curves become triangular. In this simple ECSC prototype, a considerable amount of capacitance comes from nanoporous graphene film, and the PTEPA film also provides electrochromic properties. Various ECSCs with different capacitance and electrochromic properties can be assembled through adjusting the dimensions and area of PTEPA and graphene films. For instance, a self-powered electrochromic smart window could be assembled using a PTEPA coated window glass combined with nanoporous graphene film as a window frame.

Table 1 Current density and area specific capacitance of reported electrochromic supercapatiors.

Materials based on	Current density (mA/cm^2)	Area specific capacitance (mF/cm^2)
poly(5-formylindole) (P5FIn)/WO3[10]	0.025 0.1	10.38 6.4
$WO_3 \cdot H_2O$ and Prussian white film[11]	[illegible] 0.05 1.0	[illegible] 4.87 3.67
CeO_2/TiO_2 and WO_3/PEDOT:PSS films[12]	0.05 0.3	5.3 2.1
poly(indole-6-carboxylicacid)/TiO_2	[illegible] 1.5	9.65 4.06
poly(indole-5-carboxylic acid)/WO_3[14]	0.03 [illegible]	10.11 4.40
PTEPA film and graphene film	0.015 0.03 0.06 0.12 0.3	13.3 10.9 9.2 7.2 5.3

Conclusions

In summary, the TEPA monomer was obtained through a new practical synthetic route using a safer and greener approach, and its molecular structure determined by sXRD for the first time. Its solution processable polymer PTEPA was further prepared via microemulsion polymerization. The distorted molecular structure of the TEPA monomer affects the planarity and three-dimensional conformation of the dendritic polymer PTEPA. We speculate that PTEPA has twisted channels and pores, which are narrowed and blocked by the bifurcation and distortion of PTEPA. Investigations of the microstructure of PTEPA indicate that PTEPA has a hierarchical pore structure with an average pore size of 6.8 nm. PTEPA exhibits excellent energy storage properties, as a cathode material, exhibiting a discharge capacity of 89.5 mAh/g in the initial cycle with a very sloping two-stage discharge curve and relatively stable cycling performance. Beyond excellent energy storage properties, PTEPA also shows relatively good electrochromic performance. Hence, an efficient all-solid-state ECSC prototype with good electrochromic performance and high energy storage capacity (13.3 mF cm^{-2}) was assembled based on PTEPA and nanoporous graphene films. During the charging and discharging process, the color of the ECSC changed between yellow-green and steel-blue reversibly. Thus, the energy storage level of the ECSC can be monitored by the corresponding color changes. Through adjusting the dimensions and area of the PTEPA and graphene film, various ECSCs (including self-powered electrochromic smart windows) with different capacitance and electrochromic properties might also be possible using a similar scheme. This work not only provides a new approach for the preparation of electrode materials for efficient ECSCs, but also provides an important direction for the fabrication of new electrochromic energy storage devices.

 10.1002/cssc.202000941

Experimental Section

Chemicals and Instrumentation

All reagent grade chemicals were purchased from The Aldrich or Aladdin Reagent (Shanghai) companies. Ltd., and were used without further purification. Indium tin oxide (ITO)-coated glass (sheet resistance Rs ≤ 10 Ω) was purchased from Guluo Glass Technology Co. Ltd. It was ultrasonically washed in deionized water, ethanol, acetone, toluene and (finally) ethanol solutions.

Proton (^{1}H) nuclear magnetic resonance (NMR) spectra were recorded with a Bruker Avance III instrument (Bruker, Switzerland) at 500 MHz. Fourier transform infrared (FT-IR) spectra were obtained using a Nicolet 6700 spectrometer (Thermo Fisher Nicolet, USA). Extracted ion chromatogram and mass spectra (MS) were explored using a ABSCIEX HPLC-TripleTOF 5600 Mass Spectrometer. Elemental analysis was obtained using a Perkin-Elmer 4200 elemental analyzer. Powder X-ray diffraction (pXRD) experiments were performed using a X'Pert Pro diffractometer with Cu-Kα radiation (λ= 1.5418 Å) operating at 40 kV and 40 mA and a scanning angle ranging from 5° to 50° of 2θ. Average molecular weight and polydispersity indices (PDIs) were measured through gel permeation chromatography (GPC) using a Waters Breeze 2 HPLC system. Scanning electron microscopy (SEM) images were collected using a field emission scanning electron microscope (Zeiss Gemini 300). Measurements of surface area and pore size were carried out using an ASAP 2460 surface area and porosimetry auto analyzer (Micromeritics, USA). Ultraviolet-visible (UV-vis) and near infrared (NIR) spectra were obtained using a UV-1800 spectrophotometer (Shimadzu, Japan).

Synthesis of the TEPA Monomer

As shown in Scheme 1, the TEPA monomer was obtained via a four-step synthetic route using EDOT and TPA as the starting materials in an overall yield of 55%, a detailed description of the synthetic method is provided in the ESI. Samples obtained after chromatography were shown to be analytically pure by elemental analysis (calcd for TEPA ($C_{36}H_{27}NO_6S_3$): C: H: N: S= 65.0: 4.1: 2.1: 14.4; found: C: H: N: S = 65.0: 4.1: 2.1: 14.4). ^{1}H NMR and FT-IR spectra of the obtained TEPA samples are similar to the reported spectra[31] and are shown in in Fig. S1 and Fig. S2. The +ve ion electrospray MS (Fig. S3) shows a peak at m/z = 666.1085 for $[M+H]^+$, which is very close to theoretical calculated value (666.1073).

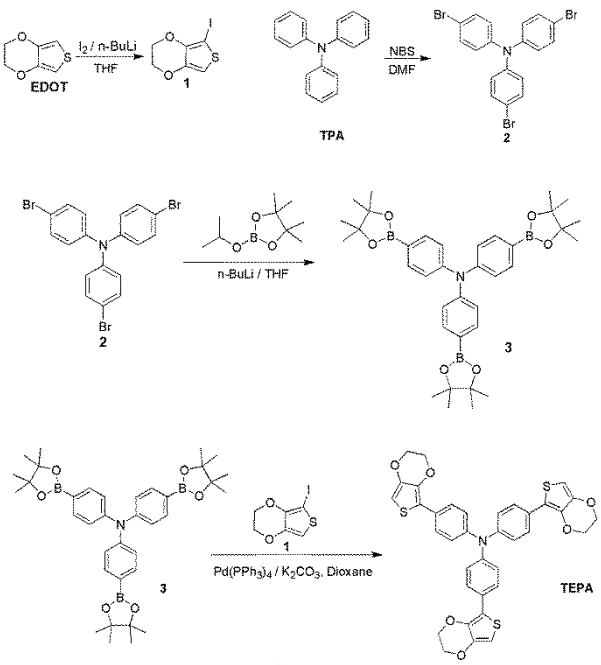

Scheme 1. The new synthetic route for the TEPA monomer.

Single-Crystal X-ray Crystal Structure Determination

Yellow sheet-like crystals of TEPA suitable for single-crystal X-ray diffraction (sXRD) measurements were grown by slow evaporation from a CH_2Cl_2/CH_3OH (1:1, by volume) solution at room temperature. sXRD analysis was carried out at T= 293(2) K on an Oxford Diffraction Gemini four-circle diffractometer, equipped with a Ruby CCD detector and using graphite-monochromatized Mo-Kα radiation. Data reduction included intensity integration, background and Lorentz-polarization correction performed with the CrysAlisPrO Version 1.171.37.35 software package (Agilent Technologies, 2014). The structures were solved by direct methods and then refined with full-matrix least-square methods using SHELXL-2014 program,[44] with all non-hydrogen atoms being refined anisotropically. A summary of the crystal data, collection parameters and refinement is given in Table 2 and selected bond lengths (Å) and angles (°) as well as hydrogen-bonding geometries are listed in Table S1 and Table S2. The dihedral angles between the two aromatic rings of TEPA molecule were calculated using the Diamond software.[45] The calculated dihedral angles are summarized in Table S3.

Table 2 Details of the structure solution and refinement of TEPA

Compound	TEPA
Chemical formula	$C_{36}H_{27}NO_6S_3$
FW	665.76
Crystal system	Monoclinic
Space group	$P2_1/c$
a (Å)	10.6825 (4)
b (Å)	15.4602 (9)
c (Å)	55.789 (3)
β(°)	93.021 (5)
V (Å^3)	9201.0 (8)
Z	12
Calculated Density (Mg/m^3)	1.442
Absorption coefficient(mm^{-1})	0.292
reflections collected	33718
independent reflections	16191 (0.076)
$R1[I>2\sigma(I)]$	0.088
*wR*2 (all data)	0.198

Polymerization of PTEPA

0.2 g dodecyltrimethylammonium bromide (DTAB) and 12 mL of 0.4 mol/L $FeCl_3$ aqueous solution were mixed and stirred for 1 h at room temperature in a two-necked round bottom flask equipped with a dropping funnel. Subsequently, the TEPA monomer (1 mmol) was dissolved in 13 mL CH_2Cl_2, which was added dropwise to the previous solution with vigorous stirring. After polymerization for 18 h, the organic phase was decanted and washed several times with distilled water to remove the organic solvent. The powder of PTEPA produced was finally washed with methanol to wash out unreacted monomer and dried under vacuum at room temperature.

Preparation and Electrochemical Measurements of PTEPA Electrodes

The PTEPA electrodes were prepared by coating a mixture containing 50% of the as-prepared PTEPA polymers, 40% acetylene black, and 10% polyvinylidene fluoride binder on circular Al current collector foils, followed by drying at 60 °C for 12 hours The load mass of the composite on the current collector was about 4 mg. After this, CR2032 coin-type cells were assembled in an argon-filled glovebox using the prepared PTEPA electrode as the cathode and lithium foil as the anode. A polypropylene micro-porous film (Celgard 2300) was used as a separator and 1 mol/L $LiPF_6$ dissolved in ethylene carbonate (EC) and dimethyl carbonate (DMC) (V_{EC}/V_{DMC}= 1:1) as the electrolyte.

Galvanostatic charge-discharge (GCD) measurements of PTEPA electrodes were carried out on a LAND CT2001A in the voltage range of 2.5-4.3 V versus Li/Li^+, using a constant current density at room temperature. Cyclic voltammetry (CV) tests were carried out in the two-electrode electrochemical cell assembled above with the scanning potential ranging from 2.5 V to 4.3 V and a scanning rate of 1 mV s^{-1} using a CHI 660E.

Preparation and Electrochemical Measurements of PTEPA Films

PTEPA powder was dissolved in chloroform to give a 1 g/L solution which was filtered through syringe filters before use, a digital photograph of this deep-blue PTEPA solution is shown in Fig. S5. PTEPA films were prepared via drop casting this solution onto ITO-coated glass substrates and drying in air at room temperature.

CV and GCD tests for energy storage performance of PTEPA films were carried out on a CHI660E electrochemistry workstation in a three-electrode system with the reference electrode being Ag/AgCl (silver wire coated with AgCl in saturated KCl solution) and the counter electrode being a platinum sheet. The electrolyte was a 1M H_2SO_4 aqueous solution. Spectroelectrochemsitry data was measured using Shimadzu UV-1800 UV-Vis spectrophotometer (Shimadzu, Japan) and Shanghai Chenhua CHI 660E electrochemical workstation in a three-electrode system with the reference electrode being Ag/AgCl, the counter electrode being a platinum wire and the electrolyte being 0.1M $LiClO_4/CH_3CN$.

Acknowledgements

We sincerely thank the support from Zhejiang Provincial Natural Science Foundation of China (No. LY19B010003) and National Natural Science Foundation of China (NSFC, No. 21501148). LR and AB also thank the Université de Strasbourg as well as the Labex CSC (Chemistry of Complex Systems) which has also supported one part of this research.

Keywords: Tris[4-(3,4-ethylenedioxythiophene)phenyl]amine • Molecular structure • Electrochromic supercapacitor • nanoporous • microemulsion

[1] P. M. Beaujuge and J. R. Reynolds, *Chem. Rev.,* 2010, **110**, 268.
[2] Y. Lv, Y. Liu, Y. Pan, G. Liu, J. Chen, Y. Guo, W. Chu, L. Shen and C. Zhang, *Chem. J. Chinese U.,* 2017, **38**, 484.
[3] A. L. Argun, A. Cirpan and J. R. Reynolds, *Adv. Mater.,* 2003, **15**, 1338.
[4] G. Liu, J. Yang, A. Bonnefont, Y. Lv, J. Chen, W. Dan, Z. Chen, L. Ruhlmann, D. S. Wright and C. Zhang, *Chem. Commun., 2018,* **54**, 14132.
[5] P. Simon, Y. Gogotsi and B. Dunn, *Science*, 2014, **343**, 1210.
[6] W. Du, Y. Lü, Z. Cai and C. Zhang, *Acta Phys.-Chim. Sin.*, 2017, **33**, 1828.
[7] W. Du, Y. Lv, H. Lu, Z. Chen, D. S. Wright and C. Zhang, *Chin. Chem. Lett.,* 2017, **28**, 2285.
[8] P. Simon and Y. Gogotsi, *Nat. Mater.,* 2008, **7**, 845.
[9] Y. Lv, W. Du, Y. Ren, Z. Cai, K. Yu and C. Zhang, *Inorgan. Chem. Front.*, 2016, **3**, 1119.
[10] Q. Guo, X. Zhao, Z. Li, D. Wang and G. Nie, *Chem. Engin. J.,* 2020, **384**, 123370.
[11] Z. Bi, X. Li, Y. Chen, X. He, X. Xu and X. Gao, *ACS Appl. Mater. Interfaces*, 2017, **9**, 29872.
[12] G. Cai, P. Darmawan, X. Cheng and P.S. Lee, *Adv. Energy Mater.*, 2017, **7**, 1602598.
[13] Q. Guo, J. Li, B. Zhang, G. Nie and D. Wang, *ACS Appl. Mater. Interfaces,* 2019, **11**, 6491.
[14] Q. Guo, X. Zhao, Z. Li, B. Wang, D. Wang and G. Nie, *ACS Appl. Energy Mater.*, 2020, **3**, 2727.
[15] a) S. Muench, A. Wild, C. Friebe, B. Häupler, T. Janoschka and U.S. Schubert, *Chem. Rev.,* 2016, **116**, 9438; b) S. Muench, A. Wild, C. Friebe, B. Häupler, T. Janoschka and U.S. Schubert, *Chem. Rev.,* 2016, **116**, 9438; b) W. Li, Y. Guo, J. Shi, H. Yu, H. Meng, *Macromolecules,* 2016, **49**, 7211; c) Y. Chen, Y. Yin, X. Xing, D. Fang, Y. Zhao, Y. Zhu, M. U. Ali, Y. Shi, J. Bai, P. Wu, C. K. Shen, H. Meng, *ChemPhysChem*, 2020, **21**, 321; d) M. A. Ochieng, J. F. Ponder, J. R. Reynolds, *Polym. Chem.*, 2020, **11**, 2173; e) S. L. Pittelli, M. D. Keersmaecker, J. F. Ponder, A. M. Österholm, M. A. Ochieng, J. R. Reynolds, *J. Mater. Chem. C*, 2020, **8**, 683; f) J. Y. Lee, S. Y. Han, B. Lim, Y. Nah, *J. Ind. Eng. Chem.*, 2019, 70, 380; g) K. Sheng, F. Xu, K. Shen, J. Zheng, C. Xu, *Electrochem. Commun.*, 2020, **111**, 106646; h) S. Ming, Z. Li, S. Zhen, P. Liu, F. Jiang, G. Nie, J. Xu, *Chem. Eng. J.*, 2020, **390**, 124572.[16] C. Su, F. Yang, L. Ji, L. Xu and C. Zhang, *J. Mater. Chem. A*, 2014, **2**, 20083.
[17] C. Su, F. Yang, Y. Ye, L. Xu, L. Wang and C. Zhang, *J. Electrochem. Soc.*, 2013, **160**, 2021.

[18] C. Su, X. Zhu, L. Xu, N. Zhou, H. He and C. Zhang, *Electrochim. Acta*, 2016, **196**, 440.

[19] a) Z. Chen, W. Li, Y. Dai, N. Xu, C. Su, J. Liu and C. Zhang, *Electrochim. Acta*, 2018, **286**, 187; b) C. Su, F. Yang, Y. Ye, L. Xu, L. Wang, and C. Zhang, *J. Electrochem. Soc.*, 2013, **160**, A2021-A2026.

[20] C. Su, H. He, L. Xu, K. Zhao, C. Zheng and C. Zhang, *J. Mater. Chem. A*, 2017, **5**, 2701.

[21] W. Li, Y. Guo, Y. Wang, X. Xing, X. Chen, J. Ning, H. Yu, Y. Shi, I. Murtazac and H. Meng, *J. Mater. Chem. A*, 2019, **7**, 116.

[22] Z. Chen, N. Xu, W. Li, R. Zhao, Y. Dong, J. Liu, C. Su, J. Wang and C. Zhang, *J. Mater. Chem. A*, 2019, **7**, 16347.

[23] Y. Dai, W. Li, Z. Chen, X. Zhu, J. Liu, R. Zhao, D. S. Wright, A. Noori, M. F. Mousavi and C. Zhang, *J. Mater. Chem. A*, 2019, **7**, 16397.

[24] H. Yen and G. Liou, *Prog. Polym. Sci.*, 2019, **89**, 250.

[25] H. Yen and G. Liou, *Polymer Chem.,* 2018, **9**, 3001.

[26] L. Ji, Y. Dai, S. Yan, X. Lv, C. Su, L. Xu, Y. Lv, M. Ouyang, Z. Chen and C. Zhang, *Sci. Rep.*, 2016, **6**, 30068.

[27] S. Kao, Y. Lin, C. Hu, M. Leung and K. Ho, *Sol. Energy Mater. Sol. Cells*, 2015, **143**, 174.

[28] H. Lin and G. Liou, *J. Polym. Sci., Part A: Polym. Chem.,* 2009, **47**, 285.

[29] X. Yang, M. Wang, J. Zhao, C. Cui, S. Wang and J. Liu, *J. Electroanal. Chem.,* 2014, **714**, 1.

[30] X. Lv, C. Huang, A. Tameev, L. Qian, R. Zhu, K. Katin, M. Maslov, A. Nekrasov and C. Zhang, *Dyes Pigm.*, 2009, **163**, 433.

[31] C. Xu, J. Zhao, C. Cui, M. Wang, Y. Kong and X. Zhang, *J. Electroanal. Chem.*, 2012, **682**, 29.

[32] X. F. Cheng, J. S. Zhao, C. S. Cui, Y. Z. Fu and X. X. Zhang, *J. Electroanal. Chem.*, 2012, **677-680**, 24.

[33] J. Zeng, Z. Wan, H. Li, P. Liu and W. Deng, *Sol. Energy Mater. Sol. Cells*, 2018, **178**, 223.

[34] X. Lv, S. Yan, Y. Dai, M. Ouyang, Y. Yang, P. Yu and C. Zhang, *Electrochim. Acta*, 2015, **186**, 85.

[35] S. Li, G. Liu, X. Ju, Y. Zhang and J Zhao, *Polymers*, 2017, **9**, 173.

[36] Y. Zhang, L. Kong, X. Liu, C. Wang and J. Zhao, *Bull. Korean Chem. Soc.*, 2016, **37**, 1234.

[37] M. Chahma, J. B. Gilroy and R. G. Hieks, *J. Mater. Chem.*, 2007, **17**, 4768.

[38] K. Idzik, J. Soloducho, M. Lapkowski and S. Golba, *Electrochim. Acta*, 2008, **53**, 5665.

[39] A. C. Albéniz and N. Carrera, Polymers for green C-C couplings, *Eur. J. Inorg. Chem.*, 2011, **15**, 2347.

[40] J. Liu, S. Mi, Z. Xu, J. Wu, J. Zheng and C. Xu, *Org. Electron.*, 2016, **37**, 169.

[41] C. Mincheol, L. Gyun, P. Byoungnam and R. Elas, *Polymers*, 2017, **9**, 212.

[42] W. Li, J. Ning, Y. Yin, X. Xing, M. Qi, T. Li, J. Cao, Y. He, I. F. Perepichka and H. Meng, *Polym. Chem.*, 2018, **9**, 5[illegible]8.

[43] Y. Yin, W. Li, X. Zeng, P. Xu, I. Murtazac, [illegible], Y. Liu, T. Li, J. Cao, Y. He and H. Meng, *Macromolecules*, 2018, **51**, 7953.

[44] G. M. Sheldrick, SHELXT - Integrated space-group and crystal-structure determination, *Acta Cryst.,* 2015, **71**, 3.

[45] Diamond - Crystal and Molecular Structure Visualization Crystal Impact - K. Brandenburg & H. Putz GbR, Postfach 1251, Gerhardstrasse 30, D-53111 Bonn.

[46] D. E. Janzen, M. W. Burand, P. C. Ewbank, D. A. Pappenfus, H. Higuchi, D. A. da Silva Filho, V. G. Young, J. Bredas and V. R. Mann, *J. Am. Chem. Soc.,* 2004, **126**, 1[illegible]95.

[47] E. Poverenov, Y. Sheynin, M. Zamoshchik, A. Patra, G. Leitus, I.F. Perepichka and M. Bendikov, *J. Mater. Chem.*, 2012, **22**, 14645.

[48] H. Hwang, Y. Kim, M. Kang, M. [illegible], Y. J. Heo and D. Y. Kim, *Polym. Chem.*, 2017, [illegible]

[49] Y. H. Wijsboom, [illegible] Patra, S. S. Zade, Y. Sheynin, M. Li, L. J. Shimon and M. Bendikov, *Angew. Chem. Int. Ed.*, 2009, **48**, 5443-5447.

[50] H. Yoon, M. Chang and J. Jang, *Adv. Funct. Mater.*, 2007, **17**, 431.

[51] B. J. Kraus and T. P. Lodge, *Polym. J.*, 2012, **44**, 131.

[52] [illegible] Jang, J. Bae and E. Park, *Adv. Mater.*, 2006, **18**, 354.

[53] L. Ren, G. Zhang, H. Li, [illegible] and S. Dou, *Int. J. Electrochem. Sci.,* 2019, **14**, 238.

[54] Z. Song, H. Duan, D. Zhu, Y. Lv, W. Xiong, T. Cao, L. Li, M. Liu and L. Gan, *J. Mater. Chem. A.*, 2019, **7**, 15801.

[55] D. Xue, D. Zhu, H. Duan, Z. Wang, Y. Lv, W. Xiong, L. Li, M. Liu and L. Gan, *Chem. Commun.*, 2019, **55**, 11219.

[56] L. Miao, H. Duan, Z. Wang, Y. Lv, W. Xiong, D. Zhu, L. Gan, L. Li and M. Liu, *Chem. Eng. J.*, 2020, **382**, 122945.

[57] X. Qian, L. Miao, J. Jiang, G. Ping, W. Xiong, Y. Lv, Y. Liu, L. Gan, D. Zhu and M. Liu, *Chem. Eng. J.*, 2020, **38[illegible]**, [illegible]208.

10.1002/cssc.202000941

Entry for the Table of Contents

Insert graphic for Table of Contents here.

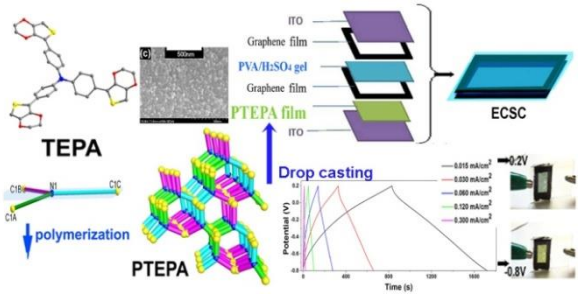

Tris[4-(3,4-ethylenedioxythiophene)phenyl]amine was obtained via a green-synthetic route and its solution-processable nanoporous polymer was used to fabricate an efficient all-solid-state electrochromic supercapacitor.